Influence of defects on the incommensurate modulation in irradiated $Ba_2NaNb_5O_{15}$

S. Barré, H. Mutka,* and C. Roucau
Laboratoire d'Optique Electronique du Centre National de la Recherche Scientifique, Boîte Postale 4347, 31055 Toulouse CEDEX, France

A. Litzler, J. Schneck, and J. C. Tolédano
Centre National d'Etudes des Télécommunications, 196 avenue Henri Ravera, 92220 Bagneux, France

S. Bouffard
Centre Interdisciplinaire de Recherche sur les Ions Lourds, Boîte Postale 5133, 14040 Caen CEDEX, France

F. Rullier-Albenque
Laboratoire des Solides Irradiés, Ecole Polytechnique, 91128 Palaiseau CEDEX, France
(Received 7 June 1990)

Defect-induced properties of barium sodium niobate ($Ba_2NaNb_5O_{15}$) have been studied as a function of electron irradiation dose. Birefringence measurements at low doses indicate that the lock-in transition temperature, originally at about 280 °C, decreases linearly with increasing dose. Complementary irradiations *in situ* in a high-voltage electron microscope show that the incommensurate phase can be stabilized down to room temperature. Simultaneously the satellite diffraction spots broaden and the lock-in transition becomes diffuse. The modification of the hysteresis of the birefringence, observed already at the lowest doses, indicates a progressive extension of the stability range of the $2q$ modulated phase to lower temperatures as the defect concentration increases. A similar conclusion can be drawn from the satellite reflection dark-field electron micrographs that show, once the incommensurate phase is stabilized at room temperature, the doubly modulated texture characteristic of the $2q$ modulated phase. Low doses of irradiation do not change qualitatively the configuration of the residual discommensurations in the lock-in phase nor the temperature dependence of the incommensurability. Accordingly, already in the as-grown samples the defects dominate the pinning of the incommensurate modulation and the intrinsic properties of this incommensurate system are not clearly observable.

I. INTRODUCTION

Numerous studies have shown that the particular properties of materials with incommensurate phases are sensitive to, or amplified by, the presence of defects.[1] In the charge-density-wave compounds $1T$-TaS_2 and $1T$-$TaSe_2$, for instance, substitutional impurities gradually stabilize the incommensurate phase on the expense of the lock-in phase and the lock-in transition can even be completely suppressed.[2] In insulating incommensurate systems, effects clearly assigned to defects have been observed too. For example, in Rb_2ZnCl_4, purified by successive recrystallizations, hysteresis phenomena are attenuated.[3] Production of defects by irradiation is another way of probing the defect-associated phenomena. It has been successfully applied in the investigation of charge-density-wave materials[4] and, more recently, also to study insulating incommensurate systems such as thiourea,[5] $[N(CH_3)_4]_2ZnCl_4$,[6] and Rb_2ZnBr_4.[7]

Barium sodium niobate (BSN), $Ba_2NaNb_5O_{15}$, is a typical example of incommensurate systems with defect-associated properties.[8] This is not surprising because the BSN crystals are nonstoichiometric with respect to the barium and sodium content. Nonstandard properties—such as the time relaxation of satellite intensities, hysteresis, incomplete lock-in phase, and memory effect—have been observed and interpreted in terms of mobile defects interacting with the modulation.[9–11] However, the most results point out that the incommensurate state is constituted by the mixing of two phases with different characteristics of modulation (see Fig. 1).[12–16] One of them is a doubly modulated ($2q$) phase and the other a unidirectionally modulated ($1q$) phase. As a consequence, the strong thermal hysteresis in BSN is likely to be associated with this coexistence of phases and not only, as it was supposed previously, with the presence of defects.

Nevertheless, defects play an important role in BSN and they probably influence the respective stabilities of the two phases. The aim of this paper is to examine the defect-induced properties of the incommensurate phase of BSN by studying the influence of new defects introduced in a controlled way by electron irradiation and to compare this influence to that of the nonstoichiometry. This is particularly interesting because BSN is one of the rare insulating incommensurate systems for which transmission electron microscopy can be used for unambiguous diffraction contrast imaging of the discommensurations[17,18] as well as for the characterization of the

TABLE I. Composition in oxides of the $Ba_2NaNb_5O_{15}$ samples. The last line gives the ideal stoichiometric composition.

Specimen	BaO (%)	Na_2O (%)	Nb_2O_5 (%)
A	38.81	9.07	52.16
B	42.03	8.30	49.67
C	41.57	8.08	50.35
ideal	40.00	10.00	50.00

phase mixtures[14,16] of the incommensurate phase. Thus, we can find out how the pinning of the discommensurations is modified in the irradiated samples and how the respective stabilities of the two incommensurate phases develop in order to define a phase diagram in presence of defects. In addition to the electron-microscopy observations that reveal the perturbations induced by the lattice defects in the structural modulation at a microscopic scale, we have carried out birefringence and electron-diffraction measurements recorded during thermal cycling the samples. These macroscopic measurements show the changes in the critical temperature of the lock-in transition and in the hysteresis phenomena.

II. EXPERIMENTAL METHODS

The BSN crystals used in these experiments come from different origins and have different compositions that are listed in Table I. Part of the electron irradiations were carried out using a 2-MeV Van de Graaff accelerator in which bulk specimens were irradiated at low doses (3.7×10^{19} to 9.3×10^{19} electrons/cm^2). These irradiations were carried out at low temperature (liquid H_2) but the samples were stored at room temperature after irradiation. For high-dose irradiations (3×10^{20} to 2.5×10^{21} electrons/cm^2) we used a high-voltage electron microscope in which limited areas, a few μm^2, of thin samples were irradiated with 2-MeV electrons at room temperature. The interest of this method is the *in situ* observation of diffraction patterns or images under irradiation. Subsequently, to the low-dose irradiations, the samples were investigated by transmission-electron-microscopy (TEM) and birefringence measurements. Electron-diffraction patterns recorded in a Philips EM400 electron microscope operating at 120 kV were used to measure the incommensurate deviation δ as a function of temperature in the range from 20 to 330 °C at the heating-cooling rate of 2.5 deg/min. Images were obtained in a JEOL 200CX electron microscope operating at 200 kV both for the samples irradiated to low doses and after the *in situ* observations at 2 MV in the high-voltage electron microscope. For all transmission-electron-microscopy observations, samples were thinned by ion beam milling before irradiation and mounted on a heating holder in order to allow observations up to 330 °C. The optical birefringence ($n_a - n_b$) was measured at the same temperature conditions as the incommensurate deviation δ. The birefringence plot is known to vary with the thermal procedure used in the experiment and is reproducible after a few cycles from room temperature up to the normal phase; so the curves presented in the following were recorded after two or three cycles.

III. INCOMMENSURATE PHASE IN THE IRRADIATED MATERIAL

The defect-creation processes and the expected fraction of displaced atoms are discussed in the Appendix. The exact concentration and nature of the stable defects is not known but we can estimate that our low-dose irradiations result in less than 0.01 dpa (displacements per atom) and that we reach 0.1–0.2 dpa at the highest doses. These estimates are upper limits. At the upper dose range, the creation of extended damage (dislocation loops, for example) could be expected but was not observed.

A. Variation of the lock-in temperature with the irradiation dose

On heating, the birefringence plot of BSN shows a linear decrease that suddenly steepens at the transition from the lock-in to the incommensurate phase. On cooling, the increase of the birefringence is less abrupt and a broad hysteresis is observed. The variation of the birefringence with temperature for a sample irradiated to different doses is shown in Fig. 2. With increasing defect concentration, the birefringence plot is clearly modified.

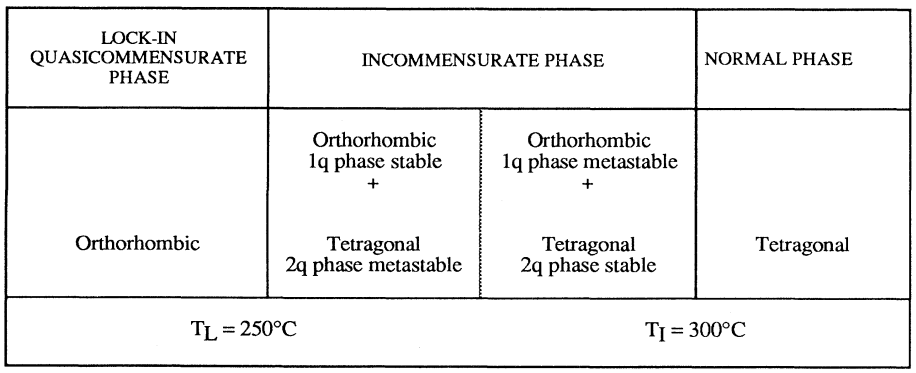

FIG. 1. Phase diagram of BSN from room temperature to 600 K in the case of a nonirradiated sample.

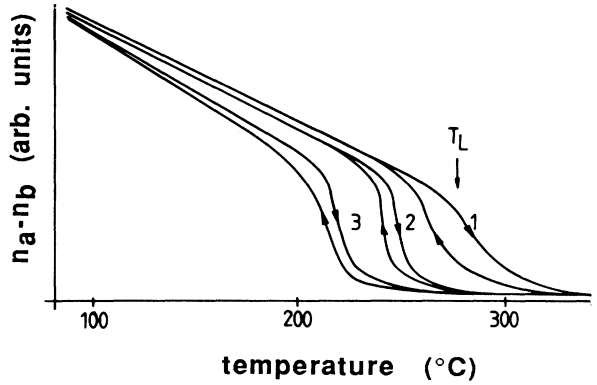

FIG. 2. Birefringence plot obtained during thermal cycling between the room temperature and the normal phase at the heating-cooling rate of 2.5 deg/min. The sample is of composition *A* and has been irradiated at 2 MeV at different doses. Curve 1 is obtained on a nonirradiated sample, curve 2 after irradiation of 4.0×10^{19} electrons/cm^2, and curve 3 after irradiation of 9.1×10^{19} electrons/cm^2.

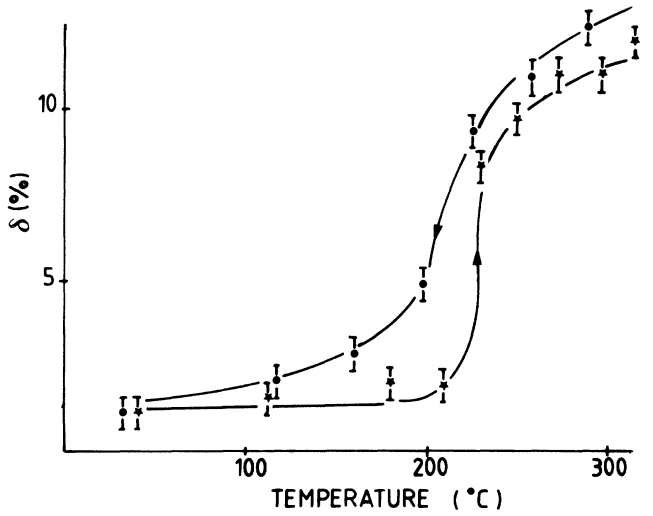

FIG. 3. The deviation from commensurate δ as a function of temperature during a cycle at 2.5 deg/min from room temperature to the normal phase obtained from an electron-diffraction experiment on a sample of composition *C* which has received an irradiation dose of 4.0×10^{19} electrons/cm^2 at 2 MeV.

The transition temperature T_L, taken at the steep deviation from the linear slope on heating, decreases by several tens of degrees due to the irradiation up to 9.1×10^{19} electrons/cm^2. Simultaneously, the form of the hysteresis cycle is modified. With increasing dose, the difference in temperature of the birefringence measured on heating and cooling cycles tends to decrease even though the total range in which the hysteresis is observed is more extended. We have repeated this experiment on another sample of different composition and the evolution with increasing defect concentration was quite similar.

The TEM investigation at room temperature reveals no difference on the satellite dark-field images and diffraction patterns between weakly irradiated samples and nonirradiated samples. The discommensuration patterns and the ferroelastic domains resemble the ones previously obtained on nonirradiated samples.[19] We have measured the incommensurability parameter δ as a function of temperature in a weakly irradiated sample (4×10^{19} electrons/cm^2). The results, presented in Fig. 3, confirm the birefringence observations. The lock-in temperature transition is lowered by about 25° compared with the value obtained on a nonirradiated sample. However, there is no noticeable modification of the shape of the hysteresis of the modulation wave vector.

The results of the experiments presented above are collected on the phase diagram in Fig. 4. We have reported the temperature of the lock-in transition T_L as a function of the irradiating dose. The three curves correspond to three samples with different compositions. T_L has been determined from birefringence experiments for curves 1 and 2 and from electron-diffraction experiments for curve 3. In irradiated samples, T_L decreases linearly as a function of the dose with the same slope in the three cases. This diagram sums up the main results concerning the extension of the range of stability of the incommensurate phase to lower temperature when the defect concentration increases in the samples. We note that, independent of the nature of the defects—intrinsic defects associated with the nonstoichiometry or irradiation defects—the lock-in temperature decreases. The upper stability limit of the incommensurate phase has not been studied in detail for the irradiated samples. The electron-diffraction data show the incommensurate satellites up to about 300 °C as do the nonirradiated samples.

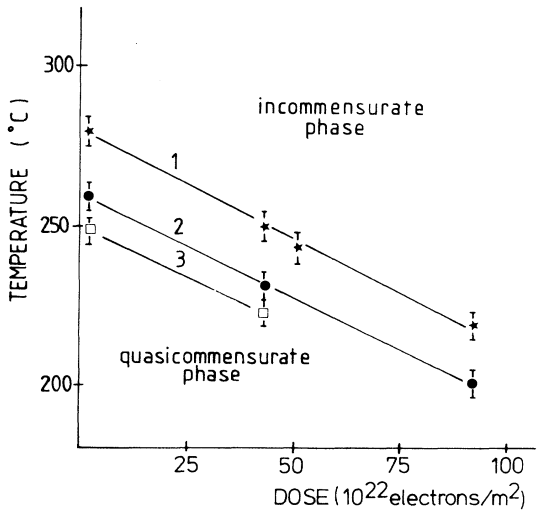

FIG. 4. Phase diagram in the presence of defects. We have reported the lock-in transition temperature T_L as a function of the irradiation dose for different samples. Curves 1 and 2 have been obtained from birefringence experiments on *A*- and *B*-type samples, respectively. Curve 3 has been obtained from an electron-diffraction experiment on a *C* sample.

The modification of the hysteresis cycle recorded during the birefringence experiments is somewhat surprising. In fact, we expected, as previously observed in irradiated thiourea, for instance,[5] an amplification of the hysteresis phenomena due to defects. On the contrary, we observe in BSN a narrowing of the hysteresis cycle. Two possible explanations can be considered. In the first place, the reason for the narrowing could be a defect-induced slowing down of the kinetics, i.e., a relaxation rate that becomes slow with respect to the time scale of the experiment, so that the system remains in the same metastable state during the temperature cycling. Actually, such an explanation was proposed in the case of the irradiated blue bronze $K_{0.30}MoO_3$ (Ref. 20) in which the hysteresis disappeared at high irradiation doses. However, in BSN another explanation appears more likely. In fact the coexistence of the $1q$ and $2q$ incommensurate phases is a natural reason for the hysteresis that then expresses the metastability of the relative proportion of the two phases. We note that the quadratic $2q$ phase does not contribute to the birefringence and so the values (n_a-n_b) is an indication of the proportion of the $1q$ phase as has been clearly demonstrated in recent experiments under uniaxial stress.[15] Accordingly, the extension of the flat region with almost zero birefringence and only little hysteresis indicates that mainly the $2q$ phase is present in the high-temperature range of the incommensurate phase. In conclusion, the birefringence results show evidence for the stabilization of the $2q$ phase in the presence of defects.

B. Further evolution of the incommensurate phase under irradiation

We have followed *in situ* in the microscope the evolution of the diffraction pattern under irradiation at room temperature. With an increasing irradiation dose, the incommensurate deviation δ increases and, as can be seen in Fig. 5, approaches values typical of the incommensurate phase (5–10 %). At doses higher than 9×10^{20} electrons/cm^2, the notable broadening of the satellite diffraction spots makes an accurate measurement of δ quite difficult. For irradiations doses exceeding 2.5×10^{21} electrons/cm^2, the satellite spots, already very diffused, disappear. Figure 6 illustrates the broadening of the incommensurate satellites with a comparison of a diffraction pattern at the beginning of the experiment and after an irradiation of about 1.9×10^{21} electrons/cm^2. In Fig. 6(b), the incommensurate parameter $\delta=(8\pm2)\%$, the uncertainty being due to the width of the spots. Another point to note is that, at the beginning of the experiment, the selected-area diffraction is that of a single ferroelastic domain. After irradiation, the two ferroelastic variants are present in the same selected area and this is also evident on the electron micrographs.

Indeed, the evolution of the images follows the evolution of the diffraction pattern as it has been previously described.[21] When the diffraction spots broaden, the contrast of the satellite dark-field images decreases, then vanishes. The micrograph presented in Fig. 7 is typical after irradiation up to a high dose (1.9×10^{21} electrons/cm^2). We observe a contrast that resembles small ferroelastic domains of the size 10 nm on average. The walls separating these domains have the directions a_t and b_t: they are marked on the micrograph. On the diffraction pattern, δ is about 6% for both of the two variants. The same complicated structure was observed in the nonirradiated material at high temperature after an annealing at 250 °C and interpreted as corresponding to the $2q$ incommensurate phase.[16] Thus, the present observation under irradi-

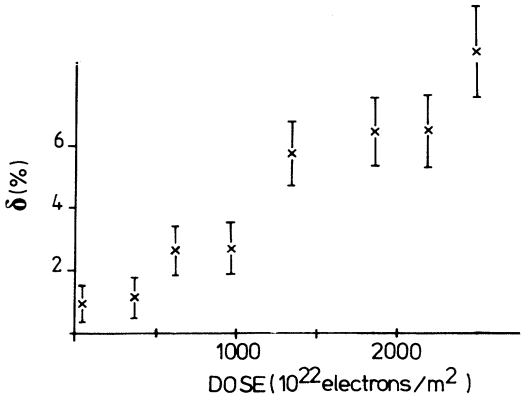

FIG. 5. The increase of the incommensurate deviation δ with the irradiation dose at room temperature. The results are collected from different samples.

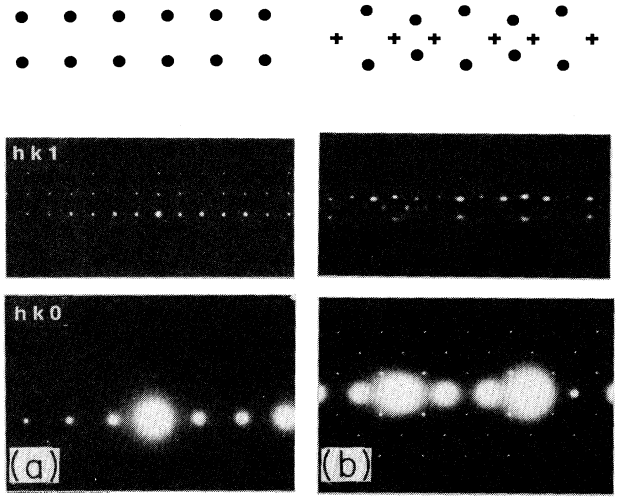

FIG. 6. Electron-diffraction patterns (a) before irradiation and (b) after irradiation at a dose superior to 1.9×10^{21} electrons/cm^2. The lower part of the patterns is the $hk0$ reciprocal plane. The upper part belongs to the $hk1$ plane that contains only satellite reflections. The modification of the weak satellite reflection pattern is schematized in an exaggerated way above the original photographs, the crosses correspond to the spots appearing due to the presence of the second variant. (a) Only one ferroelastic variant is visible in the satellite diffraction plane. δ is very low. (b) The two ferroelastic variants are now clearly visible. δ is about 6% and the satellite spots are more diffused.

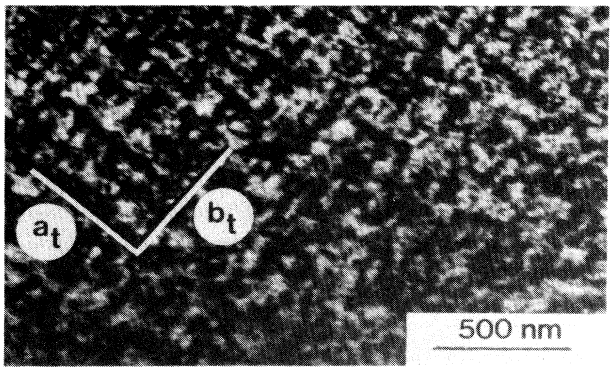

FIG. 7. The satellite dark-field image obtained at 200 kV after strong irradiation (dose $>1.9\times10^{21}$ electrons/cm^2 at 2 MeV). Note the privileged directions a_t and b_t. δ is about 6%. The corresponding diffraction pattern is presented in Fig. 6(b).

ation indicates that the $2q$ phase can be stabilized down to room temperature with a high concentration of defects. A quite recent study[22] reports on a texture typical of the incommensurate phase at room temperature after observation at high temperature (400 °C) in a 200-kV microscope. We agree with the authors of that work in relating their observation to irradiation-induced defects. However, this damage at a low incident energy is a consequence of a long irradiation time in spite of the very high incident-particle flux used in the satellite dark-field imaging conditions.

In the irradiated samples a variation with temperature of the incommensurate period is still observed. Figure 8

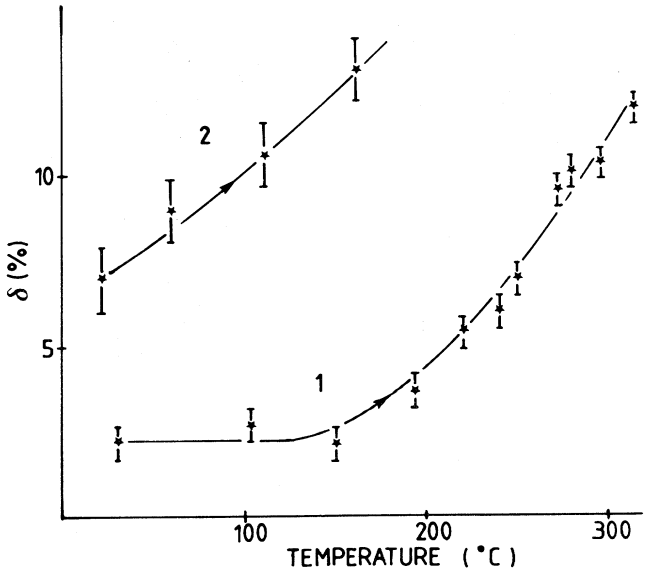

FIG. 8. Thermal variation of δ determined from an electron-diffraction experiment during a heating run at 2.5 deg/min. Sample 1 (curve 1) has received a dose of about 6.2×10^{20} electrons/cm^2; sample 2 (curve 2) has received a dose of about 9×10^{20} electrons/cm^2.

represents δ during a heating run at 2.5 °C/min in samples irradiated to high doses. Specimen 1 (curve 1) has received a dose of about 6.2×10^{20} electrons/cm^2, specimen 2 (curve 2) has received a dose of about 9.3×10^{20} electrons/cm^2. In the first case, the abrupt transition from the lock-in (constant δ) phase observed in nonirradiated samples has disappeared; the transition is now also diffuse on heating. In the second case, the error on the measurement is very important as soon as the temperature increases because of the broadening of the satellite spots and of the decrease of the diffracted intensity. δ reaches very high values (18%) but there is no lock-in transition above room temperature.

IV. DISCUSSION

Figure 9 sums up the observed phenomena. At low defect concentrations, the lock-in temperature decreases linearly with the dose; in this dose range the transition is well defined and the birefringence measurements reveal a destabilization of the $1q$ phase near the upper stability limit. At somewhat higher doses the lock-in transition becomes rather diffuse while the decrease of T_L slows down. Simultaneously, the number of residual discommensurations increases by a factor of 3–5: δ reaches values up to a few percent. At a very high dose the incommensurate phase is stabilized down to room temperature. In this dose range the TEM images and diffraction patterns show a strongly disordered incommensurate modulation that is characteristic of the $2q$ phase. Finally, the broadened satellite spots become too diffuse to be observed, indicating that the modulation disappears by losing its long-range order.

In BSN crystals the defects due nonstoichiometry with respect to the barium and sodium cations[23] are assumed to be the origin of the nonstandard effects evidenced by certain experimental results.[24] For instance, birefringence measured on off-stoichiometric samples shows that the lock-in transition temperature and the

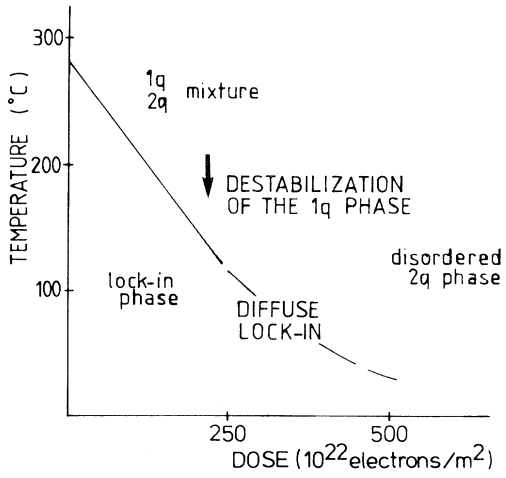

FIG. 9. Phase diagram in the presence of defects. Note the destabilization of the $1q$ incommensurate phase at the dose range where the lock-in transition disappears.

shape of the thermal hysteresis depend on the composition. X-ray precession photographs of differently prepared samples show that, at room temperature, the residual value of δ varies between 0.5 and 2 %. In the same temperature range a strong pinning of the discommensurations (DC's) can be observed at the microscopic scale, characterized by a deviation from ideal patterns.[14] Recently, it has been shown that DC's are pinned at the same placed at the beginning and at the end of a thermal cycle that extends up to the normal phase.[16] Such an observation is easy to explain if the DC's are strongly pinned by defects.

Our results confirm that the high values of δ and the low values of T_L are due to defects. A detailed correlation between T_L and δ is difficult to obtain because the measured δ is very sensitive to the thermal history of the sample. Even though the value of δ and the residual DC patterns are influenced by the defects, they are also controlled by the processes that happen at higher temperatures inside the incommensurate phase.

Indeed, the characteristic hysteresis and memory effects are observed in that temperature range and were shown to be due to the presence of $1q$ and $2q$ incommensurate phases.[16] The present results reveal how the hysteresis is modified as a consequence of a destabilization of the $1q$ phase with increasing defect concentration. At present we cannot explain in detail why the defect can favor the doubly modulated phase, especially because we ignore the atomic scale structure of the defects. However, supposing that the local chemical nature of the defects is not the dominating factor, one can argue very simply that a random defect distribution induces an isotropic strain field to which the more symmetric (tetragonal) $2q$ phase is better adapted. Slight modifications of the defect distribution can then occur in the $1q$ phase and give rise to the observed memory effect that is characterized by the phase separation.[12,14,16] Certainly this kind of picture is deviating from the original defect density wave concept[25] in details, but the general idea of accommodation between the defects and the modulation is conserved. Remarkably, a very clear difference between the $2q$ and $1q$ regions that existed in the incommensurate phase can be observed after a quench to room temperature in the lock-in phase. The former are frequently almost free of DC's ($\delta \ll 1\%$), but the latter have a relatively high disordered DC's ($\delta = 1-2\%$).[12,14,21] This can be understood considering that the slight ordering of defects that favors the unidirectional modulation also deepens the potential wells that pin the DC's. As a consequence, the elimination of DC's that necessitates a relatively long-range movement of the DC nodes becomes more difficult at the approach to the lock-in transition.

Among the effects of irradiation in BSN, the lowering of the lock-in transition temperature is typical of incommensurate systems that have been irradiated or substitutionally disordered.[1-7] It is often attributed to the ability of the incommensurate modulation to adapt more easily to the random defects because the long-range deformations of the phase cost less energy in this case. Theoretically this has been interpreted in the case of charge-density-wave compounds.[26] As a consequence of these phase deformations, the incommensurate modulation is poorly organized, as can be seen in the electron micrographs. At high enough defect concentrations the broadening of the incommensurate satellite reflections, associated with the strong phase disorder, also becomes evident, in analogy with the irradiated charge-density-wave materials.[4]

V. CONCLUSION

This electron-irradiation study has confirmed the influence of defects as a source of many unusual properties of barium sodium niobate. Irradiation at a low dose acts on the modulation in a manner analogous to the sodium vacancies existing in the nonstoichiometric samples by lowering the lock-in transition temperature. The role of defects in favoring the $2q$ phase is an important finding concerning the coexistence of two distinct incommensurate phases. It indicates that further understanding of the intrinsic properties of this incommensurate system is essential to obtain more perfect crystals. At the highest irradiation doses, phenomena typical of strongly disordered incommensurate systems are observed. These include broadening of the incommensurate satellites, softening the lock-in transition, and, finally, suppression of the lock-in phase.

ACKNOWLEDGMENTS

One of us (H.M.) wishes to thank the Academy of Finland for a travel grant for his visit to the Laboratoire d'Optique Electronique in Toulouse.

APPENDIX: DEFECT PRODUCTION

It is known that, in insulating oxides, several kinds of defect processes can occur under irradiation.[27] In general, defect production is connected to the displacement damage induced in elastic collisions with energetic particles. Electronic excitations associated with inelastic collisions can modify existing defects but do not usually create displacement damage. In any case, many different types of defects are expected and can be identified with specific methods such as optical absorption and electron paramagnetic resonance, for example. At very high irradiation doses extended defects are often observed.

In the electron irradiation of BSN the unidentified defects that influence the incommensurate phase are created by the elastic collisions. This is confirmed by our observations in the electron microscope that show an increase, by several orders of magnitude, in the damage production rate when the energy of the electrons is increased from 200 kV to 2 MV, indicating the existence of a threshold energy. Thus, Frenkel defects can be produced when the maximum energy E_m, transferred in a primary collision by an electron of energy E to an atom of mass M, exceeds a characteristic threshold value E_d. The maximum energy is given in eV by the relativistic formula[27,28]

$$E_m = 2148E(E+1.02)/M \ , \tag{A1}$$

where E is expressed in MeV and M in atomic mass units. Table II gives this energy for the four elements constitut-

TABLE II. Maximum transferred energy E_m (eV) and the displacement cross section in an elemental target σ_d (10^{-24} cm^2) for an electron of energy E to the atoms in BSN. We have taken a displacement threshold of 48 eV and cross sections for Cs and Mg, found in the tables of Oen (Ref. 33), represent Ba and Na, respectively.

	Atom	Ba	Nb	Na	O
	mass	137.5	93	23	16
E (MeV)					
2	E_m	94.4	140	564	811
	σ_d	27(Cs)	29	18(Mg)	14
0.2	E_m	3.8	5.6	22.8	32.8
	σ_d	0	0	0	0
0.12	E_m	2.1	3.2	12.8	18.4
	σ_d	0	0	0	0

ing BSN and for the different electron energies used in our experiments. The threshold energy of displacement by elastic collision is typically a few tens of electron volts; its value is usually determined experimentally once a defect has been identified. For instance, in several metal oxides the displacement thresholds are of the order of 50 eV.[29–33] Comparing with the values listed in Table II, and supposing single-element targets, we can expect that in our irradiation experiments at 2 MeV all the atoms of the structure can be displaced with cross section of the order of a few tens of barns.[34] Meanwhile, in our TEM observations at 120 or 200 kV, the theoretical probability of displacement is zero even for the light Na and O atoms. The total amount of displacements can be calculated in a polyatomic target using the tables of (Ref. 34) for the contribution of collision cascades and taking into account the secondary collisions between different atoms.[35,36] An important consequence of the mixed cascade processes is that the light atom species are displaced more efficiently than in an elemental target.[36] Accordingly, the displacement cross section can be as high as 100×10^{-24} cm^2. This means that, in our irradiations with doses ranging from 4×10^{19} up to 2.4×10^{21} electrons/cm^2, the fraction of displaced atoms varies from about 4×10^{-3} up to 0.25 dpa.

The final concentration of defects is smaller than the fraction of displaced atoms because of recombination of the vacancy-interstitial pairs created by irradiation in our samples stored at room temperature. Unfortunately, an attempt at finding an electron-spin-resonance signal associated with the irradiation-induced defects in BSN was unsuccessful and the defect concentration was not measured. For comparison we can refer to two rather similar systems. In a closely related structure, the molybdenum red bronze $K_{0.33}MoO_3$, a careful electron-spin-resonance study, helped to evaluate the number and thermal evolution of magnetic defects induced by electron irradiation.[37] A dose of 1.5×10^{19} electrons/cm^2 of 2.5-MeV electrons created a spin concentration of about 1.5×10^{20} 1/cm^3 (stable over a period of a few weeks at room temperature), corresponding to a cross section of about 40×10^{-24} cm^2. In lithium aluminate, $LiAlO_2$, electron-spin-resonance and optical studies have shown[38] that a dose of 0.8×10^{19} electrons/cm^2 gives a defect concentration of 7.7×10^{17} 1/cm^3, corresponding to a cross section of about 2×10^{-24} cm^2. This rather small value was associated with thermal recombination of defect and/or defect species not visible in the measurements. In conclusion, we expect that our irradiation experiments induce defect concentration in the range from 10^{-3} to 0.2 dpa, even less because of thermal recombination.

*Present address: Institut Laue-Langevin, 156X, 38042 Grenoble CEDEX, France.

[1]For a review, see papers in Phase Transitions **11**, 221 (1988).
[2]F. J. Di Salvo, J. A. Wilson, B. G. Bagley, and J. W. Wasczak, Phys. Rev. B **12**, 2220 (1975).
[3]K. Hamano, H. Sakata, K. Yoneda, K. Ema, and H. Hirotsu, Phase Transitions **11**, 279 (1988).
[4]H. Mutka, Phase Transitions **11**, 221 (1988).
[5]G. André, D. Durand, F. Dénoyer, R. Currat, and F. Moussa, Phys. Rev. B **35**, 2909 (1987); D. Durand and F. Denoyer, Phase Transitions **11**, 241 (1988).
[6]M. Bziouet, R. Almairac, and P. Saint-Grégoire, J. Phys. C **20**, 2635 (1987).
[7]M. A. R. Benyacar, E. Cattáneo, H. Ceva, H. Lanza, and L. Schmirgeld, Phys. Rev. B **37**, 3409 (1988).
[8]J. C. Tolédano, J. Schneck, and G. Errandonéa, in *Incommensurate Phases in Dielectrics*, edited by R. Blinc and A. P. Levanuyk (Elsevier, Amsterdam, 1985), Part. 2.
[9]J. Schneck, G. Calvarin, and J. M. Kiat, Phys. Rev. B **29**, 1476 (1984).
[10]G. Errandonéa, J. C. Tolédano, A. Litzler, H. Savary, J. Schneck, and J. Aubrée, J. Phys. Lett. **45**, L329 (1984).
[11]G. Errandonéa, J. Schneck, J. C. Tolédano, A. Litzler, H. Savary, J. Aubrée, J. M. Kiat, and G. Calvarin , Ferroelectrics **53**, 257 (1984).
[12]J. M. Kiat, G. Calvarin, and J. Schneck, Jpn. J. Appl. Phys. Suppl. **24-2**, 832 (1985).
[13]J. C. Tolédano, G. Errandonéa, J. Schneck, A. Litzler, H. Savary, F. Bonnouvrier, and M. L. Estéoule, Jpn. J. Appl. Phys. Suppl. **24-2**, 290 (1985).
[14]C. Manolikas, J. Schneck, J. C. Tolédano, J. M. Kiat, and G. Calvarin, Phys. Rev. B **35**, 8884 (1987).

[15]J. Schneck, J. C. Tolédano, G. Errandonéa, A. Litzler, C. Manolikas, J. M. Kiat, and G. Calvarin, Phase Transitions **9**, 359 (1987).
[16]S. Barré, H. Mutka, and C. Roucau, Phys. Rev. B **38**, 9113 (1988).
[17]G. van Tendeloo, S. Amelinckx, C. Manolikas, and Wen Shulin, Phys. Status Solidi A **91**, 483 (1985).
[18]Pan Xiao-Qing, Hu Mei-Shen, Yao Ming-Hui, and Feng Duan, Phys. Status Solidi A **92**, 845 (1985).
[19]S. Barré, thèse, Université Paul Sabatier de Toulouse, 1987.
[20]H. Mutka, F. Rullier-Albenque, and S. Bouffard, J. Phys. (Paris) **48**, 425 (1987).
[21]S. Barré, H. Mutka, C. Roucau, and G. Errandonéa, Phase Transitions **9**, 225 (1987).
[22]Xiaoqing Pan and Duan Feng, Phys. Status Solidi A **106**, K117 (1988).
[23]J. Schneck, Thèse d'Etat, Université de Paris VI, 1982.
[24]J. Schneck, J. C. Tolédano, C. Joffrin, J. Aubrée, B. Joukoff, and A. Gabelotaud, Phys. Rev. B **25**, 1766 (1982).
[25]J. P. Jamet and P. Lederer, J. Phys. Lett. **44**, L257 (1983); see also, J. P. Jamet, Phase Transitions **11**, 335 (1988).
[26]W. L. McMillan, Phys. Rev. B **12**, 1187 (1975).
[27]E. Sonder and W. A. Sibley, in *Point Defects in Solids,* edited by J. H. Crawford and L. M. Slifkin (Plenum, New York, 1972), Vol. 1.
[28]L. Zuppiroli, in *Défauts Ponctuels dans les Solides,* edited by G. Brebec, J. Castaing, C. Monty, C. M. de Novion, and L. Zuppiroli (les Editions de Physique, Orsay, France, 1978).
[29]G. W. Arnold and W. D. Compton, Phys. Rev. Lett. **4**, 66 (1960).
[30]Y. Chen, D. L. Trueblood, O. E. Schow, and H. T. Tohver, J. Phys. C **3**, 2501 (1970).
[31]J. M. Meese and D. R. Locker, Solid State Commun. **11**, 1547 (1972).
[32]E. R. Hodgson and F. Agullo-Lopez, Nucl. Instrum. Methods **32**, 42 (1988).
[33]G. P. Summers, G. S. White, K. H. Lee, and J. H. Crawford, Phys. Rev. B **21**, 2578 (1980).
[34]O. S. Oen, Oak Ridge National Laboratory Report No. ORNL-4897, 1973.
[35]D. Lesueur, Philos. Mag. A **44**, 905 (1981).
[36]D. Lesueur, J. Morillo, H. Mutka, A. Audouard, and J. C. Jousset, Radiat. Eff. **77**, 125 (1983).
[37]H. Vichery, F. Rullier-Albenque, and S. Bouffard, J. Phys. (Paris) **50**, 685 (1989).
[38]M. H. Auvray-Gely, A. Perez, and A. Dunlop, Philos. Mag. B **57**, 137 (1988).

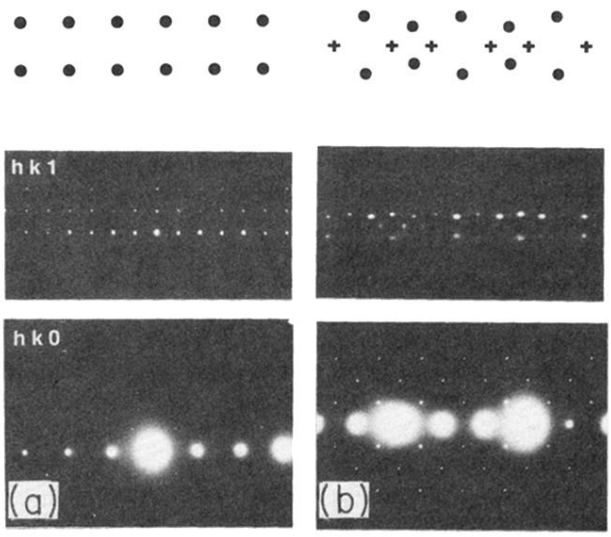

FIG. 6. Electron-diffraction patterns (a) before irradiation and (b) after irradiation at a dose superior to 1.9×10^{21} electrons/cm^2. The lower part of the patterns is the $hk0$ reciprocal plane. The upper part belongs to the $hk1$ plane that contains only satellite reflections. The modification of the weak satellite reflection pattern is schematized in an exaggerated way above the original photographs, the crosses correspond to the spots appearing due to the presence of the second variant. (a) Only one ferroelastic variant is visible in the satellite diffraction plane. δ is very low. (b) The two ferroelastic variants are now clearly visible. δ is about 6% and the satellite spots are more diffused.

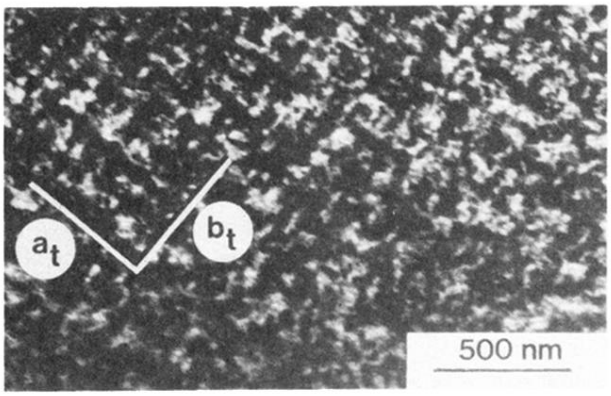

FIG. 7. The satellite dark-field image obtained at 200 kV after strong irradiation (dose $> 1.9 \times 10^{21}$ electrons/cm^2 at 2 MeV). Note the privileged directions a_t and b_t. δ is about 6%. The corresponding diffraction pattern is presented in Fig. 6(b).